ASTROBIOLOGY
Volume 7, Number 6, 2007

DOI: 10.1089/ast.2007.0075

Research Paper

Hydrothermal Systems in Small Ocean Planets

STEVE VANCE,[1,*] JELTE HARNMEIJER,[1] JUN KIMURA,[2] HAUKE HUSSMANN,[3] BRIAN DEMARTIN,[4] and J. MICHAEL BROWN[1]

ABSTRACT

We examine means for driving hydrothermal activity in extraterrestrial oceans on planets and satellites of less than one Earth mass, with implications for sustaining a low level of biological activity over geological timescales. Assuming ocean planets have olivine-dominated lithospheres, a model for cooling-induced thermal cracking shows how variation in planet size and internal thermal energy may drive variation in the dominant type of hydrothermal system—for example, high or low temperature system or chemically driven system. As radiogenic heating diminishes over time, progressive exposure of new rock continues to the current epoch. Where fluid-rock interactions propagate slowly into a deep brittle layer, thermal energy from serpentinization may be the primary cause of hydrothermal activity in small ocean planets. We show that the time-varying hydrostatic head of a tidally forced ice shell may drive hydrothermal fluid flow through the seafloor, which can generate moderate but potentially important heat through viscous interaction with the matrix of porous seafloor rock. Considering all presently known potential ocean planets—Mars, a number of icy satellites, Pluto, and other trans-neptunian objects—and applying Earth-like material properties and cooling rates, we find depths of circulation are more than an order of magnitude greater than in Earth. In Europa and Enceladus, tidal flexing may drive hydrothermal circulation and, in Europa, may generate heat on the same order as present-day radiogenic heat flux at Earth's surface. In all objects, progressive serpentinization generates heat on a globally averaged basis at a fraction of a percent of present-day radiogenic heating and hydrogen is produced at rates between 10^9 and 10^{10} molecules cm^{-2} s^{-1}. Key Words: Energy—Hydrothermal systems—Ocean planets—Rock mechanics—Tides. Astrobiology 7, 987–1005.

1. INTRODUCTION

Ice-covered moons and planets are common in the Solar System. Each of the outer planets has at least one icy moon, and the Kuiper Belt appears to contain many Pluto-sized minor planets (Brown *et al.*, 2004). Many of the larger icy moons show signs of extensive and prolonged geologi-

[1]Astrobiology Program and Department of Earth & Space Sciences, University of Washington, Seattle, Washington.
[2]Earthquake Research Institute, University of Tokyo, Tokyo, Japan.
[3]Institute of Planetary Research, German Aerospace Center (DLR), Berlin, Germany.
[4]Department of Geological Sciences, Brown University, Providence, Rhode Island.
*Present address: Jet Propulsion Laboratory, Pasadena, California.

cal activity, possibly indicating surface processes mediated by subsurface liquid water. In Mars, Europa, Callisto, Enceladus, and Titan, liquid water may persist to the present (Lyons *et al*., 2005; Zimmer *et al*., 2000; Kerr, 2005; Spohn and Schubert, 2003; Tobie *et al*., 2005a), raising the question of whether these planets host active hydrothermal systems similar to those found in Earth's oceans and whether other planets may have also done so in earlier epochs.

Of the more than 200 gas-giant planets known to circle other stars,* those with orbits beyond the frost line for their parent star may harbor icy moons. In addition, a class of larger water-bearing planets, so-called ocean planets ($M_{Earth} < M_{Planet} < 8M_{Earth}$), may be common around other stars (Leger *et al*., 2004; Raymond *et al*., 2006). Internal heating in these planets—primordial and radiogenic—would be sufficient to drive long-lived hydrothermal activity, assuming seafloor properties similar to Earth's.

Seafloor spreading caused by mantle convection is the main driver for terrestrial hydrothermal activity; 60% of Earth's internal heat is presently dissipated at spreading centers (Sclater *et al*., 1980). One might expect larger ocean planets ($M_{Planet} \geq M_{Earth}$) to drive hydrothermal systems predominantly by this mechanism as well. In ocean moons, primordial heat should be significantly less and is not likely to drive plate tectonics (McKinnon and Zolensky, 2003). In some cases tidal heating may drive mantle convection in ocean moons, but on a more limited basis than occurs on Earth, owing to their lesser internal heating.

For the purposes of this paper—considering interior processes in a variety of objects—we use the term "ocean planet" to refer to icy moons hosting subsurface liquid water, reasoning that variation of formation history among similar-sized planets and moons is probably more significant than differences in their subsequent physical evolution. We provide constraints on the depth to which fluid circulation and attending water-rock interaction occur, assuming long-term conductive cooling as the sole means for dissipating heat to the depths considered. Using these constraints, we examine the roles serpentinization-driven and tidally driven circulation may play in regulating hydrothermal activity in ocean planets. We focus on small objects—those less massive than Earth, with seafloor hydrostatic pressures less than ~200 MPa. Our model predicts the rocky mantles of these cooler and lower-pressure objects will remain brittle and thereby allow hydrothermal fluid penetration to depths greater than occur on Earth.

*As of March 2007. See http://vo.obspm.fr/exoplanetes/encyclo/catalog.php.

2. OCEAN PLANETS IN THE SOLAR SYSTEM

Oceans may have existed in the inner Solar System on Mars and Venus (Baker *et al*., 2005) and Ceres (McCord and Sotin, 2005). Subsurface water may be abundant on Mars today (*e.g*., Lyons *et al*., 2005). In the outer Solar System, the icy satellites of the giant planets and the largest trans-neptunian objects are candidate ocean planets. These objects can be divided into two groups based on size. (1) The large satellites, in which pressures are sufficient to form high-pressure ices (*e.g*., Spohn and Schubert, 2003; Tobie *et al*., 2005b) at the seafloor. This group includes Titan, Ganymede, Callisto, and trans-neptunian objects larger than about 1300 km. (2) Smaller icy satellites and trans-neptunian objects, ranging in radius from several hundreds of km up to almost 1600 km in the case of Europa, which may host oceans with water-rock interfaces (seafloors). Europa belongs to this group because of its high rock content (~90%) and the resulting high heat-production rate. Because of additional tidal heating, Europa is the most prominent known example of a small ocean planet. Other possible ocean candidates of this group include Triton, Eris (formerly 2003 UB313), Pluto, Titania, and Oberon. Oceans may be present in these objects if they are fully differentiated—a characteristic not yet determined by space missions—and if small amounts of ammonia are present to lower the melting temperature of the mixture, as is expected in the outer Solar System due to the increased abundance of volatiles in that region (Hussmann *et al*., 2006). In the largest bodies, substantial ammonia-water oceans should persist even to the present time.

Although we would not expect oceans on smaller objects today, they may have existed in the past due to the larger heating rates within the rocky component. Considering past heating adds Ariel, Umbriel, Dione, and trans-neptunian ob-

jects such as Charon, Ixion, and Quaoar to the list of possible ocean planets. For Tethys and Iapetus, the rock content is much smaller, making differentiation and oceans unlikely, even in the past. Recent Cassini spacecraft observations indicating significant internal heating in Enceladus (Spencer *et al*., 2006) highlight the possible importance of non-radiogenic energy in small icy bodies. Moment of inertia measurements for Rhea indicate the moon is nearly undifferentiated (Anderson and Schubert, 2007) and therefore unlikely to contain an ocean. Where oceans did exist, fluid-rock interactions may lead to production of heat and organic materials, as discussed below.

3. DEPTH OF FLUID CIRCULATION BELOW AN EXTRATERRESTRIAL SEAFLOOR

The possibility of a deep subsurface biota increases the space for potential habitation, especially in planets such as Mars, where traditional surface environments are verifiably hostile to known organisms (Gold, 1992). The abundance of Earth's subsurface biota is not well established but could be comparable to the surface biomass (Pedersen, 2000). Pressure, temperature, and nutrient access present challenges for putative subsurface organisms, but the ultimate limit to subsurface habitability may be access to fluid.

For the present calculations, we favor a constraint on fluid circulation depth based on thermal cracking in olivine. This approach sets an upper limit on the depth to which permeability—necessary for fluid circulation—can occur. In the next section we consider what terrestrial rock permeability can say about possible extraterrestrial hydrothermal systems.

3.1. Constraints based on the permeability of Earth's oceanic crust

Estimates of permeability in hydrothermal systems span a range from 10^{-16} to 10^{-9} m^2 (Fisher, 1998). At mid-ocean ridges and in other places where tectonic activity opens large flow channels in the seafloor, models of flow through hydrothermal systems constrain permeability to around 10^{-12} m^2 (Fisher, 1998; Fisher and Becker, 2000; Becker, 2000). Moving away from mid-ocean ridges, permeability decreases to 10^{-17} m^2 in older seafloor basalt [age ~65–200 Myr (Stein *et al*., 1995; Sinha and Evans, 2004)].

Permeability in Earth's seafloor may diminish over time due to filling of pore spaces, either by silica that precipitates from ambient fluid (Stein *et al*., 1995), or by the accumulation of sediment (Martin and Lowell, 2000). Kargel *et al*. (2000) suggest that Europa's seafloor may be covered with kilometer-thick layers of sulfate precipitates, which might promote high-temperature hydrothermal activity in a limited number of locations in the europan seafloor. Whatever the cause of diminished permeability in Earth's older seafloor, we emphasize that a broad range of permeabilities may be consistent with the other hydrothermal system parameters used by Lowell and DuBose (2005). Applying a broad range to their previous calculation suggests a number of Earth-like hydrothermal systems in a europan ocean between 10^2 and 10^8 [the number of hydrothermal systems in Earth's seafloor is estimated at 10^9 (Lowell and DuBose, 2005)].

Permeability deeper beneath the seafloor is difficult to constrain. Laboratory (Martin and Fyfe, 1970; Zimmerman *et al*., 1986) and borehole investigations (Anderson *et al*., 1985) to ~1 km depth in Earth's lithosphere indicate high temperatures and pressures tend to close pore spaces. In deep oceans such as Europa's, where average pressure at the seafloor is ~2–7 times the average in Earth's oceans (Anderson *et al*., 1998), rock permeability may be limited by high pressures. Conversely, in small bodies such as Enceladus, where core pressures approach a mere 20 MPa and where the presence of ammonia may create ocean temperatures as low as ~180 K, rock permeabilities could be much higher than those found in Earth's oceanic crust.

3.2. Constraints based on thermal cracking in olivine

In regions of ocean-ridge systems where fracture-induced large-scale permeability is absent, fluid is expected to circulate through microfracture channels in mantle rock (Lister, 1974; Sinha and Evans, 2004). A model treating the formation of microscale cracks due to thermal expansion anisotropy and mismatch (deMartin *et al*., 2004) predicts cracking depths consistent with seismic measurements indicating a transition from partially serpentinized (hydrated) to unaltered peridotite olivine at 3–4 km below the seafloor

(Canales *et al*., 2000). We apply the model to potential ocean planets in the Solar System by estimating the depth to which thermal cracking might occur (deMartin *et al*., 2004).

The lithosphere is assumed to dissipate heat through conduction, with temperature beneath the seafloor increasing with depth in proportion to thermal conductivity of mantle material [$\lambda \cong 3.0$ W m^{-1} K^{-1} for silicate rocks in Earth's upper mantle (Hofmeister, 1999)] and H_{rad}, the internal radiogenic heat below seafloor depth d (following Schubert *et al*., 1986).

Pressure below the seafloor is assumed as for a two-layer planet (Turcotte and Schubert, 1982) with core-mantle and water layer densities ρ_{mc} and ρ_w, respectively. For simplicity and for consistency with previous models of dynamics in Europa's ocean (*e.g.*, Lowell and DuBose, 2005), we choose a value for the density of water $\rho_w = 1000$ kg m^{-3}. Where the majority of the H_2O layer is frozen, ρ_w is closer to 900 kg m^{-3} (in which case we overestimate the pressure and therefore underestimate the cracking depth). In very deep oceans, near the ice III liquidus pressure, ρ_w can increase by as much 10%. The presence of salts can increase the density by a comparable amount. We choose lower-layer densities consistent with known bulk densities of the bodies under consideration. For Earth and Mars we consider the increase in pressure (P) below depth d (where hydrostatic pressure is P_d) due to overlying rock, assuming constant rock density, $\rho_m = 3500$ kg m^{-3}, and gravitational acceleration equal to the average value at the surface ($P \cong P_d + \rho_m g z$). This approach produces results for Earth's subsurface consistent with the preliminary-reference Earth model (Dziewonski and Anderson, 1981).

Because we are interested in ocean planets likely to have a water-rock interface at their seafloors, we choose the lower layer density to be greater than or equal to the average density of olivine, $\rho_m \geq 3250$ kg m^{-3}. This eliminates larger icy bodies, including Ganymede, Callisto, and Titan. We admit Enceladus to this list, but only for the maximum plausible seafloor depth of 80 km based on orbital evolution constraints (Porco *et al*., 2006); this approach is consistent with a fully differentiated moon with a hydrated rocky core (Barr and McKinnon, 2007). Other candidates are selected as discussed in Section 2, consistent with a recent survey of possible oceans in the Solar System based on thermal modeling (Hussmann *et al*., 2006).

The formation of microfractures is controlled by the development of residual stresses at grain boundaries. In a cooling aggregate, thermal expansion anisotropy between grains will increase stresses along grain boundaries. At high temperatures, residual stresses dissipate via viscous creep processes, and cracking is inhibited. At low temperatures, where dissipative processes are sluggish, residual stresses accumulate along grain boundaries. Evans and Clarke (1980) derive the following relation for the evolution of mean stress $\langle\sigma\rangle$ along a grain boundary in an aggregate cooling at a constant rate:

$$\frac{d\langle\sigma\rangle}{dT} = \frac{12\Omega D_o \delta_b E}{\sqrt{3} k_b L^3 \dot{T}} \frac{e^{-Q/RT}}{T} \langle\sigma\rangle - \frac{\beta E \Delta\alpha}{(1+\nu)}. \quad (1)$$

The first term on the right-hand side of (1) accounts for the relaxation of grain boundary stresses through viscous creep processes. The second term from the right describes the elastic contribution of grain boundary stresses owing to thermal expansion anisotropy. Individual parameters are described in Table 1.

Residual stresses begin to accumulate along grain boundaries once temperature falls below the viscous-elastic transition temperature T'. In the numerical solution to Eq. 1, T' is defined as the temperature obtained by extrapolating the elastic (linear) portion of the curve of σ versus T to zero stress. The analytical expansion solution for T' is (Evans and Clarke, 1980):

$$T' \approx \frac{Q/R_G}{\ln\left[\frac{12\Omega D_o \delta_b E}{\sqrt{3} n k_b L^3 \dot{T}}\right]}. \quad (2)$$

The normal stress σ_{yy} on a grain boundary where an elliptical flaw of size x occurs is dependent on T' and given by (Fredrich and Wong, 1986),

$$\sigma_{yy}(x) = \frac{E\Delta\alpha(T'-T)}{2\pi(1-\nu^2)} \left(\frac{4L^2}{4L^2 + (2L-x)^2} - \frac{4L^2}{4L^2 + x^2} + \ln\left[\frac{2L-x}{x}\right] - \frac{1}{2}\ln\left[\frac{4L^2 + (2L-x)^2}{4L^2 + x^2}\right] \right). \quad (3)$$

Microfractures initiate along grain boundaries when tensile stress intensity K_I exceeds a critical factor K_{IC}, a material property (also called the fracture toughness) that is independent of cool-

TABLE 1. PHYSICAL PROPERTIES USED IN THE MODEL FOR THERMAL CRACKING IN AN OLIVINE MANTLE BELOW AN OCEAN OF DEPTH d BELOW A PLANET'S SURFACE

Variable	*Vairable name*	*Value*	*Units*	*Reference*
a	Flaw size	$a < 2L$	m	
$D_o\delta_b$	Grain boundary Diffusion coefficient × Width	$1.5 \times 10^{-0.8}$	$m^2\ s^{-2}$	Hirth and Kohlstedt, 1995
d	Ocean depth below planet surface			
E	Young's modulus	197×10^9	Pa	Hirth and Kohlstedt, 1995
H	Mantle radiogenic heating		W	
k_b	Boltzmann's constant	1.38×10^{23}	$J\ K^{-1}$	
K_I	Stress intensity		$Pa\ m^{1/2}$	
K_{IC}	Critical stress intensity	0.6 ± 0.3	$Pa\ m^{1/2}$	deMartin *et al.*, 2004
L	1/2 grain size		m	
n	Fitting parameter	23		deMartin *et al.*, 2004
P_c	Confining pressure		Pa	
Q	Activation enthalpy for grain boundary	3.75×10^5	$J\ mol^{-1}$	Hirth and Kohlstedt, 1995
R	Planet radius		m	
R_G	Universal gas constant	8.314	$J\ mol^{-1}\ kg^{-1}$	
T	Temperature		K or °C	
$\dot{T}$	Cooling rate		$°C\ s^{-1}$	
T'	Viscous-elastic transition temperature		K or °C	
x	Distance		m	
z	Cracking depth below seafloor		m	
Δa	Thermal expansion anisotropy	3.1×10^{-6}	K^{-1}	Bouhifd *et al.*, 1996
β	Boundary angle	$\pi/6$	radians	
λ	Thermal conductivity	3.0	$W\ m^{-1}\ K^{-1}$	Hofmeister, 1999
v	Poisson's ratio	0.246		Hirth and Kohlstedt, 1995
Ω	Atomic volume	1.23×10^{-29}	m^3	
ρ_m	Density of mantle rock		$kg\ m^{-3}$	
ρ_w	Density of water	1000	$kg\ m^{-3}$	
σ	Stress		Pa	

ing rate. For square grains of size $2L$ with flaws ranging to size a under confining stress P_c, (Fredrich and Wong, 1986),

$$K_I = \sqrt{\frac{2}{\pi a}} \int_0^a \frac{\sigma_{yy}(x)\sqrt{x}}{\sqrt{a-x}}\, dx - P_c\sqrt{\pi a}. \qquad (4)$$

Hardness tests and measurements of the onset of permeability in hot-isostatically pressed samples indicate the critical intensity in olivine is $K_{IC} = 0.6 \pm 0.3$ MPa $m^{1/2}$ (deMartin *et al.*, 2004) (Fig. 1). Fracturing depends on confining pressure P_c, temperature difference between mantle rock and the viscous-elastic transition $T' - T$, and grain size $2L$. We use this model to find the depth of thermal cracking, z, for grain sizes between 100 μm and 10 mm. We note that larger grain sizes may be expected in regions of extraterrestrial seafloors that have cooled more slowly than observed regions on Earth's seafloor.

The cracking front is calculated for a given cooling rate ($\dot{T}$) and grain size ($2L$) by setting $K_I = K_{IC}$ and finding corresponding pressures and temperatures in Eq. 4. Maximum flaw size a is determined from the maximum of the curve of K_I versus a—that is, we assume once K_I exceeds K_{IC} for a given flaw size a, a full-grain boundary crack forms. Cracking is expected to occur to some extent for $K_I < K_{IC}$ due to factors not considered here [such as corrosion and non-standard rheology at high temperatures (Atkinson, 1984)], and in this sense our model underestimates the depth of cracking. For the present application we assume a bulk cooling rate of $\dot{T} = 1°C\ yr^{-1}$ where cracking occurs, consistent with cooling rates at mid-ocean ridges. Inhomogeneities in seafloor heating and composition will lead to variation in cooling rate, but the dependence on cooling rate is weak, as discussed below.

The method for finding cracking depths is illustrated in Figs. 2, 3, and 4. Applying this analysis in regions of Earth's seafloor where mantle material is exposed (so-called metamorphic core complexes), with $\dot{T} = 1°C\ yr^{-1}$, yields a cracking depth of 0.5 km for 100 μm grains and 6 km for 1 mm grains, where seafloor depth d is taken to be 4 km and radiogenic heating H_{rad} is 3.1×10^{13}

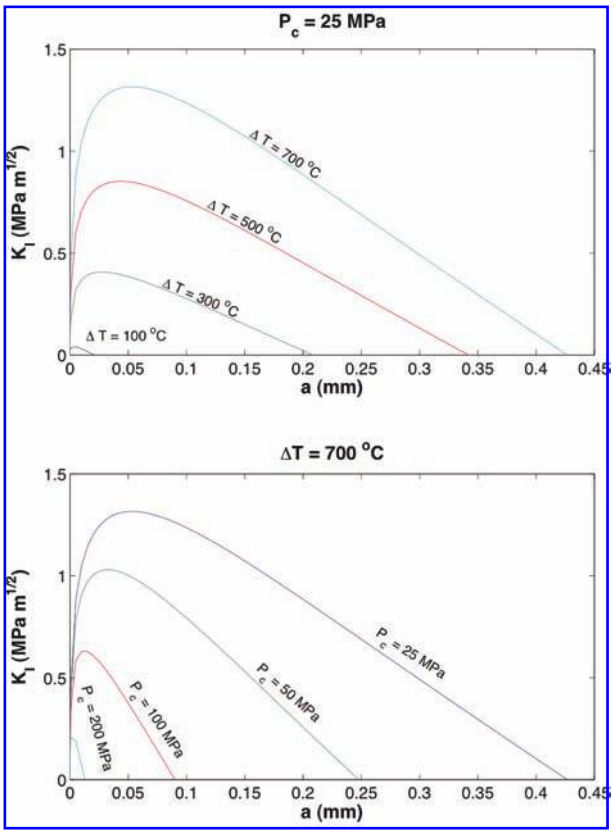

FIG. 1. Stress intensity K_I in olivine with 1 mm grain size (L = 0.5 mm) as a function of maximum flaw size a for a range of temperatures at 25 MPa, and for a range of pressures at 700°C [corrected from deMartin *et al.* (2004), Fig. 6]. For a given set of P_c and T, a is chosen from the maximum of the curve in the iterative calculation of P_c and T corresponding to the critical stress intensity (K_{IC}).

W in the current era. This result is consistent with the depth of transition to unaltered peridotite in the MARK area of the Mid-Atlantic Ridge inferred from seismic measurements (Canales *et al.*, 2000).

Earth's internal heat is predominantly dissipated at spreading centers driven by mantle convection; it is likely unique among ocean planets in the Solar System in this respect. In cooler objects unable to sustain mantle convection, internal heat may be dissipated uniformly by conduction or by localized melting in the mantle (Lowell and DuBose, 2005). Cooling is likely slower in extraterrestrial lithospheres. The effect on cracking depth is difficult to determine; slower cooling reduces cracking depth (by roughly a factor of four going from $\dot{T}$ = 1°C yr^{-1} to $\dot{T}$ = 1°C Gyr^{-1}) by allowing cracks to heal, but larger grain sizes increase cracking depth (by a factor of roughly two, dependent on planet size and ocean depth, going from 1 mm to 10 mm grains) by magnifying the accumulation of cooling-induced stress.

A lower bound on cooling rate is obtained from the change in a planet's geotherm as internal heating from long-lived radionuclides diminishes over time. In this model, water may be continuously exposed to fresh rock as a planet cools. Present rates of penetration (dz/dt) are given in Table 2 for fifteen potential and known ocean planets, assuming grain size 1 mm and cooling rate $\dot{T}$ = 1°C yr^{-1}. During the first ~4 Gyr, dz/dt is initially lower by 50%, while the interior is very hot, and then higher by about 20%. In all objects considered, the rate of exposure of new rock is one to ten thousand times slower than present rates of seafloor spreading on Earth (45 mm yr^{-1}). Possible implications for hydrothermal activity are discussed below.

Also notable is the effect of diminished internal heating on the depth of cracking, z (Table 2). Where cooling rate, grain size, and grain composition are identical to those for the regions of Earth's seafloor under consideration, fluid circulation is predicted to occur to orders of magnitude greater depth. Revised depths of fluid circulation would change previous estimates of the biopotential of extraterrestrial lithospheres (see Section 5.2).

4. SOURCES OF HYDROTHERMAL ENERGY

As on Earth, igneous rocks likely to dominate the ocean floors of icy planets may be rich in ferromagnesian silicates (olivine and pyroxene) that equilibrated at high temperatures. The characteristic temperature and cooling rates of a planet depend on the environment in which it formed—for example, whether the protoplanet thermally equilibrated in the insulating shroud of the solar nebula (or planetary subnebula for icy satellites)—and the initial inventory of radiogenic elements it incorporated. Table 2 lists estimates of present-day heating for eleven known and possible ocean planets in the Solar System (Schubert *et al.*, 1986). Figs. 3 and 4 illustrate where the different sources of heat are generated and highlight the different length scales relevant to terrestrial planets and icy bodies. In this section we discuss other sources of energy potentially important in extraterrestrial hydrothermal systems.

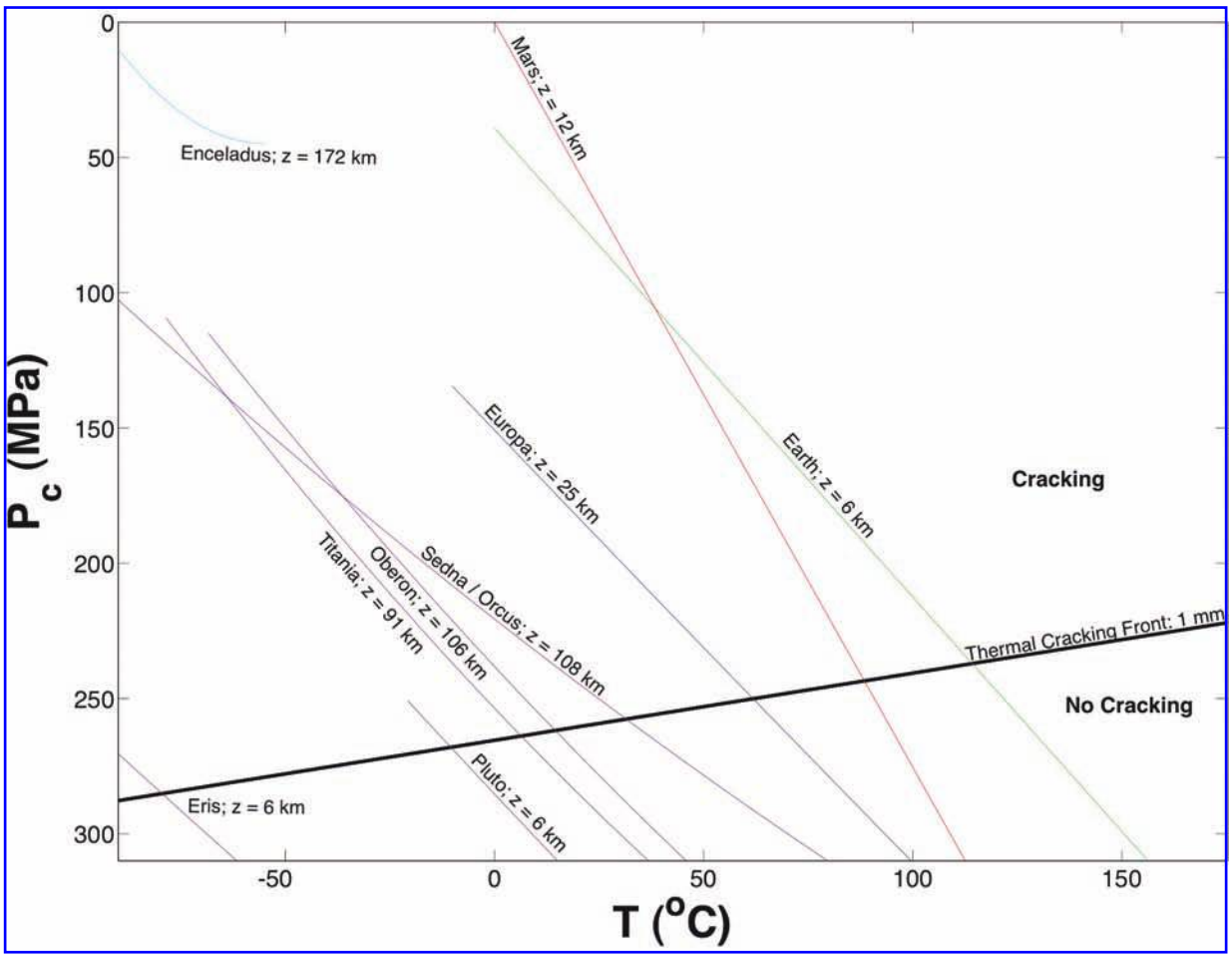

FIG. 2. Pressure-temperature profiles in planetary seafloors. Temperature (in °C) is plotted versus confining pressure P_c for a two-layer object starting at seafloor depth z shown next to each object's name. Thermal cracking is predicted to occur to critical pressures and temperatures depicted here for olivine with 1 mm grain size, assuming a critical stress intensity of 0.6 MPa $m^{1/2}$ and a cooling rate of 1°C yr^{-1}. Corresponding cracking depths are noted for each object, as determined by locating the intersection of a given geotherm with the cracking front. Estimates for Earth, Mars, Europa, and Enceladus are based on available constraints on mass distribution (ocean depth, density, and moment of inertia; see text and Figs. 3 and 4). Cracking depths are estimated for other candidate water-bearing objects in the Solar System as determined by Hussmann *et al*. (2006), assuming the minimum ammonia concentration (which determines T at the seafloor) necessary to support an ocean.

4.1. Tidal heating

Tidal interaction between a satellite and its primary is relevant to the satellite's ocean-rock interface in two ways: (1) energy is dissipated due to tidal flexing and (2) the tidal bulge of the ice shell and ocean induces pressure changes at the seafloor because of mass loading. The first of these can in some cases contribute significantly to the satellite's energy budget. The latter process generates only modest heating for generous estimates of rock porosity. However, tidally enhanced fluid flow may be important where thermal gradients are not steep enough to drive vigorous convection.

4.1.1. Heat from tidal deformation

Tidal deformation and corresponding dissipation rates will be high for large satellites on eccentric orbits close to their primaries. In the case of synchronously rotating satellites in low-eccentricity orbits, the heating rate is given by (Segatz *et al*., 1988)

$$H_{tidal} = \frac{21}{2} R^5 n^5 \frac{e^2}{G} Im(k_2), \qquad (5)$$

where R is the satellite radius, n is the orbital mean motion, e is the orbital eccentricity, and G is the constant of gravitation. $Im(k_2)$ is the imaginary part of the potential tidal Love number k_2

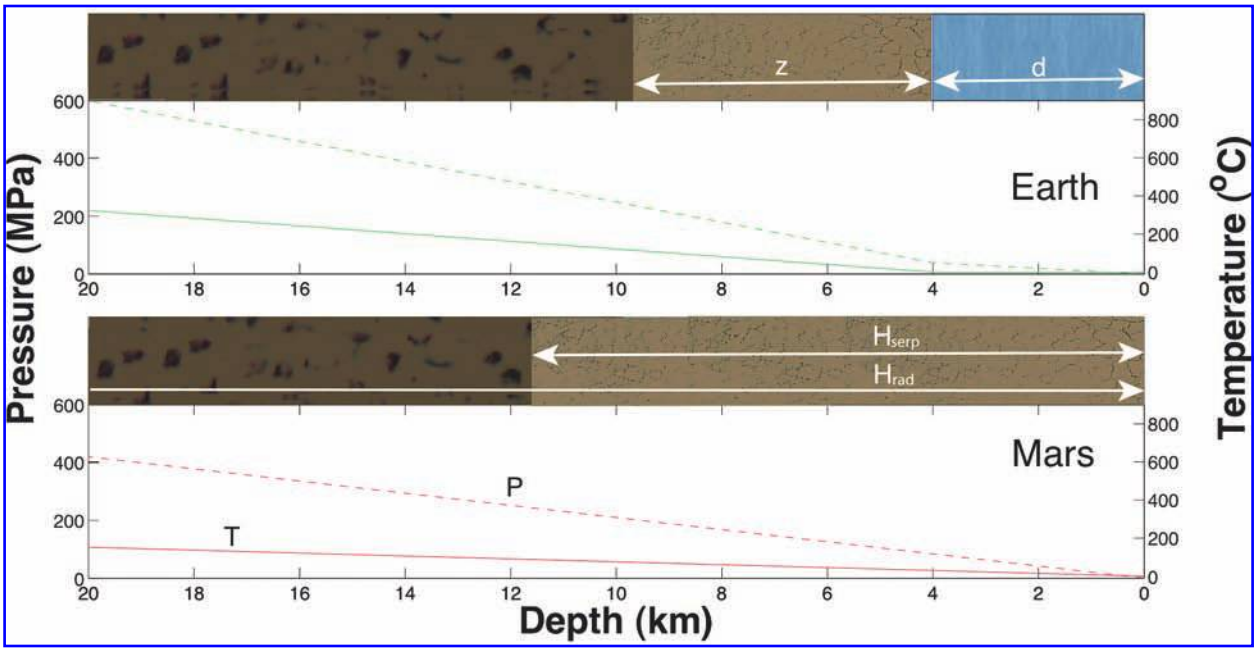

FIG. 3. Near-surface pressure, temperature, and cracking depth profiles for Earth and Mars. Cracking occurs to depth z in an olivine mantle below an ocean of depth d (for Mars, $d = 0$), assuming material parameters as given in Table 1. For these two objects, pressure is calculated from surface gravity. Temperature is calculated for a conducting seafloor based on estimated radiogenic heating H_{rad}. For any choice of cooling rate and grain size, a martian crust of the same composition as Earth's has twice the cracking depth. Further results and implications are presented in Sections 4 and 5 for the current epoch, assuming nominal grain size and cooling rate for mid-ocean ridges on Earth.

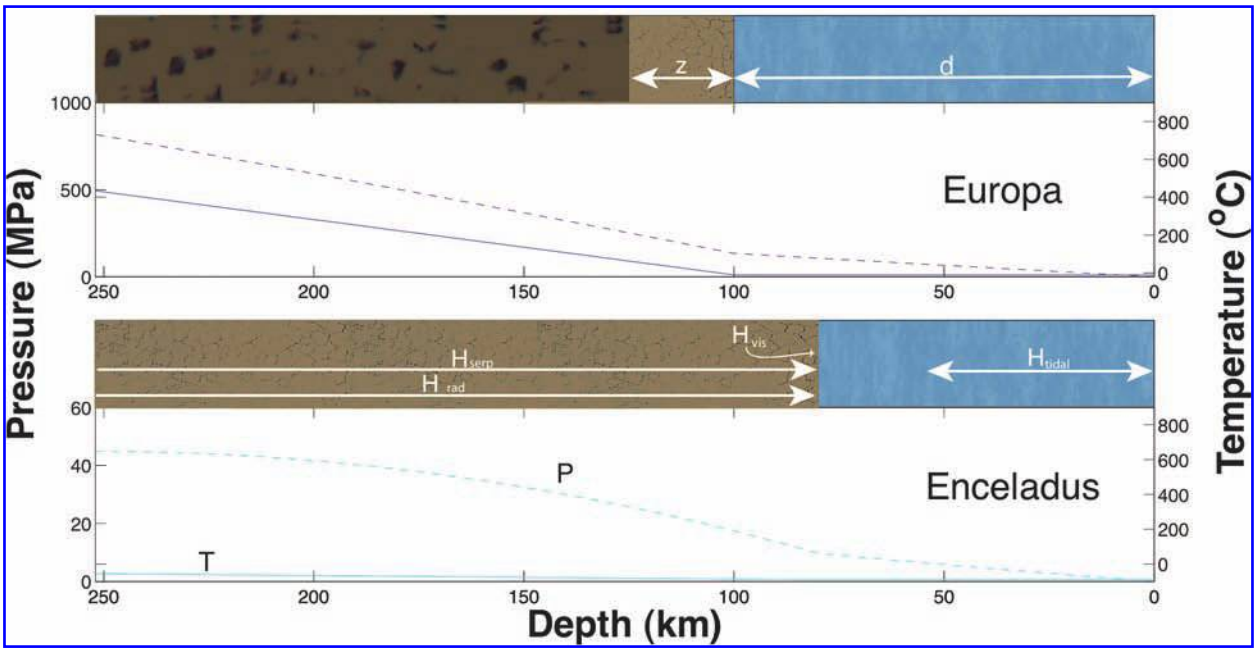

FIG. 4. Pressure, temperature, and cracking depth profiles for Europa and Enceladus. Cracking occurs to depth z in an olivine seafloor below an ocean of depth d, assuming material parameters as given in Table 1. For all icy planets considered, pressure is calculated for a two-layer object with an upper layer of depth d and density $\rho_w = 1000$ kg m^{-3} and lower layer density consistent with available bulk planetary value. Temperature is calculated for a conducting seafloor based on estimated radiogenic heating H_{rad}. Seafloor temperature is assumed to be at the melting temperature of a likely ocean composition—salt water for Europa and ammonia/water for Enceladus. Varying seafloor depth for Europa over the range of present constraints (Anderson *et al.*, 1998), z changes from 31 km for $d = 80$ km to $z = 5$ km at the maximum depth of $d = 170$ km. Shown above is the cracking depth for $d = 100$ km, for which $z = 25$ km. For very deep oceans, hydrostatic pressure limits the extent of cracking. Thus, Ganymede, Callisto, Titan, and Triton are not considered here. Further results and implications are presented in Sections 4 and 5 for the current epoch, assuming nominal permeability, grain size, and cooling rate for mid-ocean ridges on Earth.

evaluated at the surface. The latter is defined as the ratio of the tidal potential due to the displacement of mass inside the satellite (formation of the bulge) to the potential due to the external perturber. The imaginary part of k_2 is a measure for the tidal phase lag or, equivalently, the relaxation time due to inelasticity of the satellite's material (ice or rock). Here we assume a viscoelastic Maxwell model to calculate the tidal response of the satellites, assuming dissipation occurs only in an ice layer overlying a liquid water ocean.

We calculate the heating rates according to Eq. 5 for all the satellites that may contain oceans. For the rigidity and viscosity of ice-I we assume 3.3 GPa, and 5×10^{15} Pa s, respectively. Exceptions are Enceladus and Europa. For Enceladus we adjusted (lowered) the viscosity in order to match the internal heating constraint of 6 GW, which was derived from Cassini data (Spencer *et al*., 2006) as Enceladus's energy release in the south polar region. For Europa we assumed an ice thickness of 30 km and a viscosity of 5×10^{14} Pa s, which would be consistent with previous structure and tidal heating models. Dissipation in all the models is assumed to occur due to inelasticity of the ice shell. The results are given in Table 3.

The height of the tidal bulge (radial displacement u_r) can be calculated from the radial Love number h_2, as

$$u_r = \frac{h_2 \phi}{g}, \tag{6}$$

where g is the gravitational acceleration at the satellite's surface and ϕ is the potential due to the primary, evaluated at the satellite's surface. The potential depends on the longitude and co-latitude of the point considered at the surface, and on time, because of the varying distance of the satellite resulting from its orbital eccentricity. Expressions for the potential are given by Segatz *et al*. (1988) and Moore and Schubert (2000). Inserting the potential into Eq. 6 and calculating the maximum height of the tidal bulge (which will be located at the equator) yields the values given in Table 3.

If heated by radiogenic heating alone, Enceladus is not predicted to host an ocean presently. Recent Cassini measurements suggesting strong internal activity (Porco *et al*., 2006; Spencer *et al*., 2006) indicate an ocean may exist in this moon. We thus assume a typical internal structure model including an ocean (see caption, Table 3) to calculate the tidal deformation and dissipation

Table 2. Thermal Cracking Depth and Related Hydrothermally Relevant Properties for Earth and Other Possible Ocean Planets (Past and Present)

	R_p *(km)*	M_p *($\times 10^{20}$ kg)*	d *(km)*	T_o *(°C)*	T_z *(°C)*	P_z *(MPa)*	z *(km)*	dz/dt $\left(\frac{mm}{yr}\right)$	H_{rad} $\left(\frac{mW}{m^2}\right)$	$\frac{H_{serp}}{H_{rad}}$ *(%)*	F_{H_2} $\left(\frac{F}{F_\oplus}\right)$
Earth	6371	59742.00	4	0	114	237	6	0.000	60.59	0.00	1
Mars	3397	6420.00	0	0	88	243	12	0.000	22.87	0.01	1
Europa	1565	487.00	100	−10	62	250	25	0.001	8.77	0.05	4
Enceladus	252	0.73	80	−90	0	45	172	0.000	0.61	6.56	32
Titania	789	35.27	269	−69	14	262	91	0.004	2.75	0.43	12
Oberon	761	30.14	280	−79	6	264	106	0.005	2.41	0.52	13
Pluto	1195	131.40	365	−21	−10	268	6	0.000	5.10	0.02	1
Charon	604	16.20	159	−90	97	241	256	0.027	2.19	0.91	21
Eris	1300	172.00	386	−90	−80	285	6	0.000	5.50	0.02	1
Sedna/Orcus	800	40.00	238	−90	31	258	108	0.007	3.38	0.51	17

R_p and M_p are equatorial radius and mass, respectively. Seafloor depth (d) is chosen from best presently known values compatible with the existence of an olivine mantle. For potential ocean planets in the outer Solar System (lower portion), depths are taken from Hussmann *et al.* (2006) for a minimum initial ammonia concentration consistent with the existence of a liquid layer at temperature T_o. Depth of thermal cracking (z) below the seafloor in the current era is given for an olivine matrix composed of 1 mm grains cooling at a rate of 1°C yr^{-1}. T_z and P_z are temperature and pressure at depth z. dz/dt represents the rate of increase in cracking depth (in mm yr^{-1}) in the current era (seafloor spreading on Earth is currently 45 mm yr^{-1}). Corresponding surface heat flux (H_{serp}) is given as a percent of radiogenic heating (H_{rad}). Per-unit-area molecular hydrogen flux (F_{H_2}) is normalized to Earth's value of 10^9 molecules cm^{-2} s^{-1}. For Enceladus, fluid access is predicted to occur to the deepest interior in the earliest period. Heat and H_2 fluxes for Enceladus are averaged over the moon's presumed 4.5 Gyr history. Fluid-rock interactions may continue to the present in Enceladus where low-temperature kinetics limit rapid reaction, or if tidal processes cause episodic high-temperature alteration of the interior (see Section 4.1.1.).

for Enceladus. Note that a heat production rate based on our simple choice of ice thickness and ice viscosity may not necessarily represent a steady state in which the heat production will be in equilibrium with the heat flow through the ice shell. To search for equilibrium states requires detailed modeling of possible temperature profiles and the resulting heating rates, which would be beyond the scope of this paper. In the case of Enceladus the values are chosen to be consistent with the heat release observed by Cassini. They do not describe a thermal equilibrium state for Enceladus.

As shown in Table 3, significant tidal heating can be expected on Europa and Enceladus. For all other bodies considered here, heating will be less than 1% of the total heat budget. Radial displacement at the satellites' surfaces (u_r) is about 27 m on Europa, a few meters for Enceladus, and a few tens of cm for Triton. With an order of only a few cm or less, u_r is negligible (but non-zero) for the other objects considered here.

Tidal heating rates mainly depend on the orbital eccentricity. That value is in general expected to have been even greater in the past because it is usually damped by dissipation within the satellite, a process occurring on a timescale of billions or, at a minimum, millions of years. Thus, the present-day value for tidal dissipation may be representative of most of a satellite's history. One exception occurs when the orbital eccentricity of a satellite is forced by that of another due to a mean motion resonance. Io, Europa, and Ganymede share a 4:2:1 resonance. Enceladus is locked in a 2:1 resonance with Dione. Where resonances occur, orbital eccentricities may be forced to non-zero values depending on the nature of the resonance. Coupling with the satellites' thermal states may lead to oscillation of the orbital elements with time. The phenomenon may have important consequences for the heat budgets of satellite systems (Hussmann and Spohn, 2004), but full consideration in the present context is left for future work.

4.1.2. Heat generated by tidally induced porous flow

Tidal deformation of the ice shell covering a liquid water ocean acts as a time-varying hydrostatic head. This pumping action may induce fluid-rock interactions at the seafloor. Pressure at the seafloor varies with the periodic change in tidal loading. This drives fluid circulation through fractures in the mantle rock. Depending on the physical characteristics of the seafloor, viscous interaction between the fluid and the rock may generate heat sufficient to drive chemistry important for life. The amount of dissipation depends on the elastic properties of fluid and rocky matrix, the tidal period, and the amplitude of the tidal deformation. From the values for the tidal deformation given in the previous section, only the ice layers of Europa and Encelandus experience significant tidal deformation (Table 3). Here we estimate the heat generated by this tidally induced porous flow for Europa.

Wang and Davis (1996) estimated Earth's tidal dissipation by fluid flow in subsea formations for an M2 tide with an amplitude of 1 m and period of 12 hours. We follow their model, applying the tidal amplitudes given in Section 4.1.1. The dissi-

Table 3. Tidal Dissipation Rate (H_{tidal}) and Maximum Radial Displacement at the Surface (u_r) for Satellites in which Oceans Might Exist

	k_2	h_2	Im (k_2)	H_{rad} ($\times 10^9$ W)	H_{tidal} ($\times 10^9$ W)	H_{tidal}/H (%)	u_r (m)
Europa	0.242	1.169	0.0054	198	2870	94	27.4
Enceladus	0.066	0.177	0.0036	0.256	5.00	95	3.8
Titania	0.034	0.096	0.0025	9.26	0.0024	0.25	0.07
Oberon	0.028	0.076	0.0032	7.34	$\sim 10^{-4}$	~ 0	0.008
Triton	0.163	0.555	0.0052	69.40	0.17	0.25	0.24

The internal structure models and the radiogenic heating rates due to long-lived isotopes H_{rad} are taken from Hussmann *et al.* (2006). H_{tidal} and u_r are calculated from Eqs. 5 and 6, respectively. H_{tidal}/H is the ratio of tidal heating and the total heating rate $H = H_{tidal} + H_{rad}$. Values for Enceladus are calculated assuming an ice thickness of 5 km and an ice viscosity of 10^{15} Pa s, yielding the Cassini-derived output of energy (Spencer *et al.*, 2006) of about 6 GW. For Europa, we assume an ice layer thickness of 30 km and an ice viscosity of 5×10^{14} Pa s. For the remaining satellites we assume an ice viscosity of 5×10^{15} Pa s. For Triton we assume an eccentricity of e = 0.0004 (Murray and Dermott, 1998).

pation energy is the product of the Darcy flow velocity and pressure gradient. Fluid velocity through a porous matrix, or Darcy velocity, is given by

$$w = -\frac{\kappa}{\mu}\frac{\partial p}{\partial z}. \tag{7}$$

where κ is the permeability, μ is the fluid viscosity, taken to be 10^{-3} Pa s, p is the incremental pressure change, and z is the depth. The pore pressure change below the seafloor is governed by the following equation, assuming that a seafloor medium consists of L layers and the flow is mostly vertical,

$$\frac{\partial^2 p_j}{\partial z^2} = \frac{1}{n_j}\left(\frac{\partial p_i}{\partial t} - \gamma_j \frac{\partial \sigma_B}{\partial t}\right). \tag{8}$$

where $j = 1, \cdots, L$, p is the incremental pressure change, z is the depth, and t is the time. The loading function for the ocean tide is $\sigma_B = \sigma_b \cos(2\pi t/\tau)$, where $\sigma_b = \rho_w g u_r$, and τ is the tidal period (for Europa, $\tau = 3.55$ days). The elastic properties of seafloor material are described by the bulk modulus of the matrix frame, pore water, and solid grains, denoted by K, K_f, K_s, respectively, and the Poisson's ratio ν of the frame. Transport properties depend on the permeability κ, the porosity n, and the fluid viscosity μ, which is taken to be 10^{-3} Pa s. The pressure wave due to tidal fluctuation propagates to a characteristic depth controlled by the hydraulic diffusivity $\eta = \kappa/\mu S$ during the tidal period. The depth of cracking to which the water can percolate is greater than this characteristic scale (as illustrated in Fig. 4 and Table 2). S is the storage coefficient of the saturated porous medium, which describes the effect of compressibility of the seafloor components. The storage coefficient is $S = (1/K') + (n/K_f)$ if the solid materials are assumed incompressible compared to the matrix frame and pore fluid $(1/K_s \cong 0)$ (van der Kamp and Gale, 1983). In this case , the loading efficiency is given by (Jacob, 1940),

$$\gamma = \frac{1}{1 + n\,(K'/K_f)}, \tag{9}$$

where K' is the horizontally confined bulk modulus of the matrix frame related to K and ν. Details of other parameters are described in Wang *et al*. (1999). In a single near-surface layer ($L = 1$ in Eq. 8), the energy generated by tidally driven viscous dissipation can be approximated as

$$H_{vis} = \frac{\sigma_b^2}{2}\sqrt{\frac{\pi\kappa}{\mu\tau K'\gamma}}\,(1-\gamma)^2. \tag{10}$$

Material parameters are taken to be the same as Earth's—that is, we use $v = 0.25$, $K_f = 2.2$ GPa (Turcotte and Schubert, 1982). For the present calculations we choose a range of values for Earth's seafloor: frame bulk modulus K' is between ~0.1 GPa for the seafloor sediments and ~10 GPa for solid rock (Crone and Wilcock, 2005). Figure 5 shows energy dissipation per unit area as a function of the confined frame bulk modulus K' and permeability κ for a porosity of $n = 0.1$ as a maximum value, consistent with drill hole measurements in the upper 1000 m of Earth's oceanic crust (Becker *et al*., 1982). For permeability ranging from 10^{-16} to 10^{-9} m^2, as mentioned in Section 3.1, and $K' = 10$ GPa, heating from viscous dissipation (H_{vis}) is on the order of 0.001 to 1 mW m^{-2}. Heat generation varies by roughly an order of magnitude in the range of porosities between 0.1 and 0.9 (Fig. 6). Assuming these material properties for the bodies under consideration, this heating mechanism is significant only in Europa because the height of the tidal bulge in other satellites is quite small (Table 3). For example, even assuming unrealistically high porosity of $n = 0.5$ and $\kappa = 10^{-10}$ m^2, the heat generation due to tidally induced porous flow in Enceladus, Titania, Oberon, and Triton is 5.02×10^{-4}, 1.99×10^{-6}, 1.78×10^{-8}, and 1.20×10^{-4} mW m^{-2}, respectively, which are one or more orders of mag-

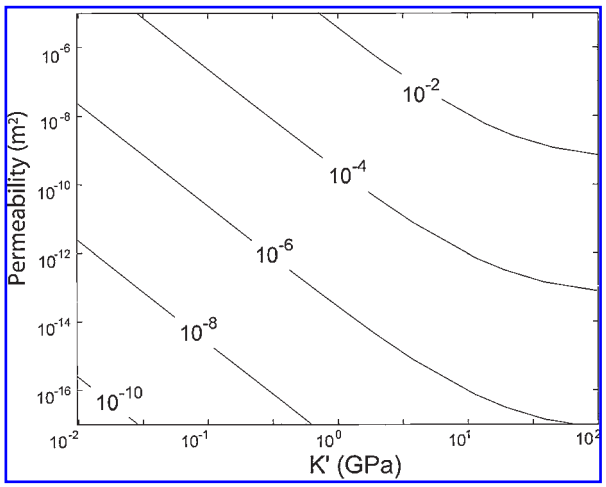

FIG. 5. Rates of tidal energy input (W m^{-2}) from viscous dissipation in the near subsurface of Europa's seafloor as a function of the permeability and the confined bulk modulus of the matrix frame K' with a reference porosity of $n = 0.1$ (Becker *et al*., 1982).

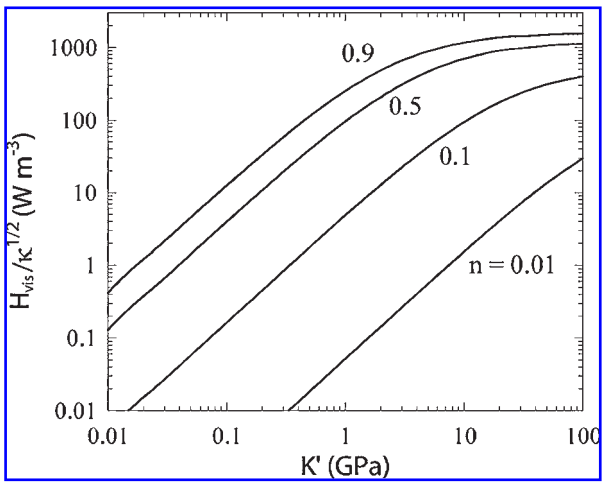

FIG. 6. Viscously dissipated energy H_{vis} normalized to permeability in a europan seafloor with tidal height u_r = 27.4 m, and Poisson's ratio ν = 0.25, for a range of porosities from n = 0.01 to 0.9.

nitude smaller than radiogenic heating rates (see Table 2). The same values of K', n, and κ yield heat generation in Europa of about 5.8 mW m^{-2}, comparable with the radiogenic heating rate.

In reality, the seafloor has spatially heterogeneous elastic properties. Where interfaces separate vertical seafloor layers with different bulk moduli, additional porous flow is induced by the difference in instantaneous response of the pore pressure across the interfaces. This effect can be approximated as a two-layer system ($L = 2$ in Eq. 8)—an interface dividing two uniform half-spaces with contrasting frame bulk moduli. Around the interface, the same order of magnitude of energy dissipation as in the case of a single near-surface layer ($L = 1$ in Eq. 8) is generated. If the seafloor has multiple-layered structure with different bulk moduli, the amplitude of generated heat may become several times larger Wang *et al*. (1999). Although this effect deserves further investigation, the relative paucity of data and the large uncertainties in the parameters suggest that more detailed discussions are unlikely to be important here. The present discussion illustrates a potential importance of viscous dissipation in generating heat in Europa's seafloor.

4.2. Serpentinization

At the off-axis mid-Atlantic hydrothermal systems Trans-Atlantic Geotraverse (TAG), Rainbow, and Lost City, the geological process of serpentinization provides a significant source of thermal energy. In the Lost City system it very likely constitutes the dominant source (Kelley *et al*., 2005). We consider the potential for serpentinization processes in extraterrestrial oceans lacking mid-ocean-ridge tectonics, with implications for astrobiology.

Ferromagnesian silicate minerals are dominant in unfractionated igneous rocks (*e.g*., peridotites) that comprise Earth's upper mantle and may typify subseafloor lithologies on small ocean planets. The abundance of peridotite in a planetary lithosphere is largely governed by the temperature of formation, which depends on the timing of formation relative to the body's ability to dissipate heat (Schubert *et al*., 1986; McKinnon and Zolensky, 2003). Even later, slower radiogenic heating can be intense enough to form peridotite, but eventually cooling takes over and the system turns retrograde—at lower temperatures, thermodynamic equilibrium favors a transformation back to the hydrated mineral form, in this case serpentine. In the event of an early period of peridotite-forming intense heating, the subsequent formation of an ocean or oceans could give rise to an epoch of serpentinization-driven hydrothermal activity.

The process of serpentinization essentially acts to re-equilibrate peridotitic assemblages from a nascent water-deficient high-temperature state to the water-saturated low-temperature state characterizing planetary seafloor environments. In the presence of water, the common rock-forming silicate minerals olivine and clinopyroxene, at the pressures under consideration (10–200 MPa) and at temperatures less than ~700 K, occur within the stability field of the serpentine minerals (antigorite, lizardite, and chrysotile). The resultant metamorphic hydration reaction is termed "retrogressive," as it accompanies a decrease in metamorphic grade. Such reactions are typically accompanied by both a large molar solid volume increase ($\Delta V_{solids} > 0$) and the release of heat energy ($\Delta H_{reaction} < 0$). The heat released is appreciable: at 300 K and pressures between 10 and 200 MPa, for example, ~83 kJ of heat is released per mole of serpentine produced. Within the pressure-temperature window pertinent to serpentinization on small ocean planets, which lies entirely within the stability field of serpentine, the exothermic nature of the reaction increases with temperature and decreases weakly with pressure.

Of additional significance is the large positive solid volume change associated with serpentinization. This is of particular interest to the crusts of ocean planets because of the potential feedback resulting from increased exposure of serpentinizable peridotitic material through crack propagation and kernel formation (O'Hanley, 1992), following the initial onset of serpentinization. The change in volume of the solid during serpentinization (ΔV_{solids}) is a function of pressure and temperature, and in the pressure-temperature window considered lie between 45 and 60 cm^3 per mole of serpentine produced. An important consideration on the volumetric expansion, however, is the rate of peridotite dissolution relative to serpentine precipitation. If dissolution is fast relative to precipitation and to the rate of migration of the alteration fluid, volumetric expansion and heat production may be inhibited (Nesbitt and Bricker, 1978).

An estimate of the heat generated by serpentinization is obtained by considering the energy released in hydrating available material in the volume of rock to depth z below the seafloor. The per-unit-area heat for a reaction penetrating to depth z is determined from an estimate of the amount of olivine produced by the reaction $H_{hydration} = n_{oliv}\Delta H/A_{seafloor}$. In our heat calculations, we consider the reaction for the Mg-end member,

$$2Mg_2SiO_4 + 3H_2O \longleftrightarrow Mg(OH)_2 + Mg_3Si_2O_5(OH)_4 \quad (11)$$

$$\text{forsterite} + \text{water} \longleftrightarrow \text{brucite} + \text{serpentine}.$$

Although the thermodynamics of the reaction will differ along the geothermal gradients considered, the dependence on pressure and temperature is trivial compared to other considerations. For simplicity we assume an average enthalpy of reaction of $\Delta H = -83$ kJ per mole serpentine. We assume a lherzolitic bulk composition consistent with Earth's primordial mantle: 70% olivine, with an Fe/Mg ratio of 0.1. We assume all of the olivine is hydrated to serpentine.

Our estimates for presently known and candidate ocean planets are given in Table 2, with tidal and radiogenic heating for comparison. Heat due to serpentinization comprises less than one percent of radiogenic heat for all bodies considered. However, as we discuss in the following sections, centers of serpentinization may drive the production of bionutrients. The slow release of this form of energy allows it to sustain gradients in chemical potential over long periods of time. These factors make even minor amounts of serpentinization important when assessing habitability.

4.3. Longevity of serpentinizing systems

The rate at which serpentinization reactions proceed potentially plays a large part in determining the longevity of hydrothermal systems on small ocean planets. Many factors affect the rate of serpentinization. These include pressure, temperature, fluid composition (as indicated by, *e.g.*, pH, Eh, CO_3^{2-}, and silica activity), fluid access to serpentinizable rock, and the Fe/Mg ratio of the peridotitic material undergoing serpentinization. Reaction rate constants determined in the laboratory (*e.g.*, Martin and Fyfe, 1970; Wegner and Ernst, 1983) are on the order of 10^{-7} to 10^{-8} sec^{-1}. Such rapid rates would preclude the persistence of hydrothermal systems on geological timescales. However, rates so determined apply to experimental systems with very fine grain sizes and a high fluid/rock ratio, conditions that become increasingly unrealistic with depth of fluid penetration. Under conditions more relevant to the crusts of small ocean planets, fluid delivery to the rock is more likely to be the rate-determining factor. In such cases, a much slower reaction rate between 10^{-11} and 10^{-13} sec^{-1} is applicable (Skelton *et al.*, 2005). In the absence of crustal rejuvenation, these reaction rates imply longevities of hydrothermal systems on the order of 10^6 years. Accordingly, serpentinizing systems may have been short-lived phenomena in planetary systems lacking tectonism and crustal rejuvenation, as all available serpentinizable material would have hydrated within the first million years of ocean/crust interaction. Given that the inception of life on Earth likely occurred rapidly after the formation of a stable lithosphere (Rosing, 1999), and the possibility of a hydrothermal cradle for life (Brasier *et al.*, 2002; Van Kranendonk, 2006), such early periods of serpentinization may be of considerable interest to astrobiology.

There are two reasons why serpentinizing systems may survive for extended periods in ocean planet crusts: (1) serpentinization in small ocean planets may occur at lower temperatures than those observed in serpentinizing hydrothermal

systems on Earth. At 298.15 K, the rate of olivine dissolution in the laboratory ranges from 10^{-11} to 10^{-17} mol cm^{-2} s^{-1} (Wogelius and Walther, 1992); (2) our estimates suggest that crack propagation and resulting exposure of fresh serpentinizable peridotitic material to fluid proceed at rates on the order of 1 km Ga^{-1}. This slow serpentization can proceed provided fluids can reach deep, fresh rock through the already serpentinized layer.

4.4. Serpentinization as a source of nutrients and metabolites

Irrespective of their potential as a source of thermal energy, serpentinizing systems are of considerable astrobiological relevance to small ocean planets (*e.g.*, Zolotov and Shock, 2003, 2004). The interaction of seawater with peridotite leads to significant change in fluid compositions, with potentially important implications for astrobiology. Unfortunately, flux measurements of potential metabolites in systems on Earth are hampered by the difficulty of distinguishing serpentinization-derived solutes from those of a magmatic origin.

In addition to heat, H_2, and CH_4, serpentinizing systems may also provide a source of biologically important trace metals. On Earth, elevated fluid concentrations of Mn, Fe, Co, Ni, Cu, Zn, Ag, Cd, Cs, and Pb have been ascribed to the serpentinization of ultramafic rocks (Douville *et al.*, 2002), although the pH dependence of such leeching processes is not well constrained.

Water in equilibrium with serpentinizing peridotite is characterized by a high pH and highly reducing conditions (Schroeder *et al.*, 2002; Wetzel and Shock, 2000). This theoretical finding is not always compatible with observations in the environment (*e.g.*, Moody, 1976; Seyfried and Dibble, 1980; Janecky and Seyfried, 1986; Allen and Seyfried, 2003). Allen and Seyfried (2004) argue that this unexpectedly high pH is a transient phenomenon resulting from the preferential hydration of the relatively siliceous pyroxene component following the initial onset of serpentinization. Lower pH increases concentrations of Fe, Ni, Cu, Zn, Ca, and K (Charlou *et al.*, 2002) in hydrothermal fluids.

4.4.1. H_2 generation

The highly reduced nature of molecular hydrogen (H_2) makes it a candidate electron donor in chemotrophic metabolic processes such as methanogenesis. The production of H_2 is of further astrobiological interest due to the potential, in the presence of CO and/or CO_2 and an appropriate catalyst, for the abiological production of another important electron donor, CH_4 (Berndt *et al.*, 1996; Charlou *et al.*, 1998) by the overall reaction:

$$4H_2 + CO_2 = CH_4 + 2H_2O \quad (12)$$

H_2 generation in serpentinizing systems has been demonstrated in the field (Neal and Stanger, 1983; Abrajano *et al.*, 1990; Kelley and Früh-Green, 2001), in the laboratory (Janecky and Seyfried, 1986; Berndt *et al.*, 1996; McCollom and Seewald, 2001) and theoretically (Wetzel and Shock, 2000; Sleep *et al.*, 2004).

The release of H_2 in serpentinizing systems results from Mg and Fe^{2+} partitioning in the products of serpentinization reactions that is markedly different from that in the protolith ferromagnesian silicates. This occurs because serpentine and brucite tend to incorporate relatively lower amounts of Fe(II) into their structures than do the reactants olivine or pyroxene. Oxidation of the unincorporated Fe(II) originally hosted in fayalite and/or ferrosilite, via dissociation of water, produces magnetite and hydrogen gas, giving rise to the net reactions (Allen and Seyfried, 2003):

$$3Fe_2SiO_4 + 2H_2O = 2Fe_3O_4 + 3SiO_2(aq) + 2H_2(aq) \quad (13)$$

fayalite + water = magnetite + silica + hydrogen

$$3FeSiO_3 + H_2O = Fe_3O_4 + 3SiO_2(aq) + H_2(aq) \quad (14)$$

ferrosilite + water = magnetite + silica + hydrogen

The amount of H_2 released through serpentinization thus depends upon the degree of Fe-incorporation into the secondary assemblage. Of central importance to evaluating H_2 fluxes on small ocean planets, therefore, is the composition of the protolith assemblage that undergoes serpentinization. Ultramafic (peridotitic) versus basaltic assemblages and higher Fe/Mg ratios in the protolith assemblage favor higher H_2 production during serpentinization.

In terrestrial systems, approximately two-thirds of the Fe(II) originally present in fayalite is

oxidized to magnetite (Berndt *et al*., 1996). The stoichiometry of the main H_2-producing reaction (Eq. 13) suggests that 3 moles of fayalite produce 2 moles of hydrogen. Hydrogen from subseafloor serpentinization may be a limiting nutrient in ocean moons that support life. For the reaction of forsterite (Eq. 11) Allen and Seyfried (2003) observe 2.3 mmol kg^{-1}. The reaction of fayalite (Eq. 13) produces ~500 mmol kg^{-1}, as estimated for the Coast Range ophiolite (Schulte *et al*., 2006).

5. IMPLICATIONS FOR LIFE IN OCEAN PLANETS

We estimate rates of heat and hydrogen production through time using our constraints on circulation depths based on thermal cracking (Section 3.2). After one billion years, rates are nearly constant; everywhere, the global heat generated by hydrating to the cracking depth is at most a percent of radiogenic heating. Hydrogen production is $\sim 10^9$ molecules per cm^2 per second for Pluto, Eris, Earth, Mars, and Europa, and $\sim 10^{10}$ molecules per cm^2 per second for the other bodies listed in Table 2. Our estimates of heat and hydrogen production in small ocean planets can be compared with emerging evidence of methane in the Solar System and with previous calculations of potential extraterrestrial biomass production.

5.1. Organics in the Solar System

Cosmochemical observations are beginning to reveal a plethora of organic molecules in gaseous nebulae outside the Solar System (Pendleton and Allamandola, 2002). To date, only methane has been observed on any of the objects discussed here (not counting Earth). However, there is reason to expect larger organic molecules where methane is found. In this section, we highlight some recent observations of methane in the Solar System as a possible indication of other organic molecules. We wish to emphasize that the processes outlined in this work may aid in the production of organics in small ocean planets.

Methane has been detected in the atmosphere of Mars (Formisano *et al*., 2004). Calculated residence times point to a source from isolated locations on the martian surface (Krasnopolsky, 2005). The majority of the martian methane is likely created by abiotic Fischer-Tropsch reactions associated with serpentinization (Oze and Sharma, 2005). In the case that all of the observed methane is abiogenic, the observation methane is nevertheless an important indication of possible nutrients for life on Mars (Fisk and Giovannoni, 1999; Weiss and Ingersoll, 2000).

Pluto and Eris are the first trans-neptunian objects with measured methane reflectance spectra (Delsanti and Jewitt, 2006). The four-hour rotation rate of recently discovered trans-neptunian object 2003 EL_{61}, as revealed by light curve measurements, constrains the object's density to between 2600 and 3340 kg m^{-3} (Rabinowitz *et al*., 2006), implying it is primarily a rocky body with a superficial covering of ices. As with other trans-neptunian objects, the tidal-orbital evolution of 2003 EL_{61} and its satellites is not yet constrained (Brown *et al*., 2005), and may be a source of energy to drive chemical weathering of the body's interior.

Methane observed on distant icy objects may derive partially from retrogressive metamorphism. The rocky components of trans-neptunian objects and small icy satellites such as Enceladus may be fully accessible to water owing to their small sizes. Tidal interactions in binary and multiple-object systems provide an additional source of energy and possibly a means for driving fluid flow. As such, trans-neptunian and other icy "dwarf planets" should not be dismissed as targets of potential astrobiological interest.

5.2. Potential extraterrestrial biomass

Estimates of the potential for supporting life geochemically on Earth or elsewhere vary depending on the temperatures, pH, and reactions considered (Shock, 2004; McCollom and Shock, 1997, 1998; McCollom *et al*., 1999). For Mars and Europa, estimates of biologically available energy from volcanic activity and from weathering reactions indicate that the number of bacteria that could be supported over a 4 Gyr period is ~8.6 g cm^{-2} on Mars—at least a hundred times less than on Earth in one thousand years—and far fewer on Europa (Jakosky and Shock, 1998; Link *et al*., 2005). Based on material presented here, we suggest there is reason to rethink these estimates. First, the cited estimates do not account for subsurface weathering as a source of energy. Jakosky and Shock (1998) suggest that weathering ~5% of crustal material to 10 km depth would contribute an additional factor of 20 to potential biomass production, but they choose to neglect this

factor because at such depths permeability sufficient to support fluid circulation is deemed unlikely. We advocate that it is at least plausible that weathering occurs not only at depth but at depths even greater than the 10 km suggested for Mars.

Second, additional energy from the sources considered here must also be taken into account, assuming that some portion of the heat they produce is converted to bioavailable nutrients. Viscous tidal dissipation could be an important source of additional heat in ice-covered moons such as Europa and Enceladus if tidal flexing occurs primarily in an ice shell overlying a liquid ocean. Serpentinization ultimately derives from other sources of energy via initial dehydration of parent rock, much of it likely coming from an early stage in a planet's history when conditions may have been too hot to support life. In this way, serpentinization-driven systems may offer a way for organisms to reclaim primordial heat energy.

6. CONCLUSION

Owing to a greater depth of hydrothermal circulation from thermal cracking in brittle mantle material, small ocean planets in the Solar System may have the capacity to support ecosystems that are stable on geologic timescales, with greater amounts of bioavailable energy than previously suggested. Unreacted rock may be exposed at a steady rate as the thermal cracking front moves deeper into the lithosphere due to the decrease in internal radiogenic heating. Based on this constraint, present-day depth of water penetration for Mars may be roughly an order of magnitude greater than previous estimates. If oceans exist in Europa, Enceladus, Titania, Oberon, and Triton, the tidal bulge of their ice shells may drive hydrothermal fluid flow if sufficient permeability exists below their seafloors. In Europa, an estimate of viscous heating from fluid flux through a porous matrix indicates heating by this mechanism may be on the same order as present radiogenic heating. In Enceladus, the presence of a subsurface ocean may facilitate tidal heating in the overlying ice shell on the same order as present-day radiogenic heating, a result consistent with heat release derived from Cassini spacecraft measurements (Spencer *et al*., 2006). It should be noted that there is no evidence for a global ocean from present Cassini data. However, to obtain high heating rates within the ice shell of Enceladus, a decoupling from the interior is required. Whether local liquid reservoirs would allow for sufficient tidal heating remains to be investigated.

In satellites locked in tidal resonances, crustal rejuvenation is possible if orbital resonance oscillations occur. Without such rejuvenation, the slow deepening of cracks over time, as outlined above, provides a steady source of thermal and chemical energy that may be sufficient to maintain stable, if limited, ecosystems to the current era.

ACKNOWLEDGMENTS

This project was supported by the National Science Foundation's IGERT program, grant number DGE-9870713, "IGERT: Astrobiology: Life in and beyond Earth's Solar System," NSF award EAR-0337796, the NASA Astrobiology Institute, and NASA award NNG06GF81G. We thank William Brazelton for discussion on the biochemistry of hydrothermal systems, Bernard Evans for helpful discussions on serpentinization thermodynamics, and Tim Crone for helpful comments on tidal dissipation. We thank the reviewers for their helpful critiques.

REFERENCES

Abrajano, T., Sturchio, N., Kennedy, B.M., Muehlenbachs, K., and Bohlke, J.K. (1990) Geochemistry of reduced gas related to serpentinization of Zambales Ophiolite, Philippines. *Appl. Geochem.* 5, 625–630.

Allen, D.E. and Seyfried, W.E. (2003) Compositional controls on vent fluids from ultramafic-hosted hydrothermal systems at mid-ocean ridges: an experimental study at 400 degrees C, 500 bars. *Geochim. Cosmochim. Acta* 67, 1531–1542.

Allen, D.E. and Seyfried, W.E. (2004) Serpentinization and heat generation: constraints from Lost City and Rainbow hydrothermal systems. *Geochim. Cosmochim. Acta* 68, 1347–1354.

Anderson, J.D. and Schubert, G. (2007) Saturn's satellite Rhea is a homogeneous mix of rock and ice. *Geophys. Res. Lett.* 34, L02202.

Anderson, R.N., Zoback, M.D., Hickman, S.H., and Newmark, R.L. (1985) Permeability versus depth in the upper oceanic crust: *in situ* measurements in DSDP hole 504B, eastern equatorial Pacific. *J. Geophys. Res.* 90 B5, 3659–3669.

Anderson, J., Schubert, G., Jacobson, R., Lau, E., Moore, W., and Sjogren, W. (1998) Europa's differentiated internal structure: inferences from four Galileo encounters. *Science* 281, 2019–2022.

Atkinson, B.K. (1984) Subcritical crack growth in geological materials. *J. Geophys. Res.* 89, 4077–4114.

Baker, V.R., Dohm, J.M., Fairen, A.G., Ferre, T.P.A., Ferris, J.C., Miyamoto, H., and Schulze-Makuch, D. (2005) Extraterrestrial hydrogeology. *Hydrogeology Journal* 13, 51–68.

Barr, A.C. and McKinnon, W.B. (2007) Convection in Enceladus' ice shell: conditions for initiation. *Geophys. Res. Lett.* 34, L09202.

Becker, K. (2000) Seeding the oceans with observations. *Oceanus* 42, 2–5.

Becker, K., Von Herzen, R.P., Francis, T.J.G., Anderson, R.N., Honnorez, J., Adamson, A.C., Alt, J.C., Emmermann, R., Kempton, P.D., Kinoshita, H., Laverne, C., Mottl, M.J., and Newmark, R.L. (1982) *In situ* electrical resistivity and bulk porosity of the oceanic-crust Costa Rica Rift. *Nature* 300, 594–598.

Berndt, M.E., Allen, D.E., and Seyfried, W.E. (1996) Reduction of CO_2 during serpentinization of olivine at 300 degrees C and 500 bar. *Geology* 24, 351–354.

Bouhifd, M.A., Andrault, D., Fiquet, G., and Richet, P. (1996) Thermal expansion of forsterite up to the melting point. *Geophys. Res. Lett.* 23, 1143–1146.

Brasier, M.D., Green, O., Jephcoat, A., Kleppe, A., Van Kranendonk, M., Lindsay, J., Steele, A., and Grassineau, N. (2002) Questioning the evidence for Earth's oldest fossils. *Nature* 416, 76–81.

Brown, M.E., Trujillo, C., and Rabinowitz, D. (2004) Discovery of a candidate inner Oort cloud planetoid. *Astrophys. J.* 617, 645–649.

Brown, M.E., Bouchez, A.H., Rabinowitz, D., Sari, R., Trujillo, C.A., van Dam, M., Campbell, R., Chin, J., Hartman, S., Johansson, E., Lafon, R., Le Mignant, D., Stomski, P., Summers, D., and Wizinowich, P. (2005) Keck Observatory laser guide star adaptive optics discovery and characterization of a satellite to the large Kuiper Belt object 2003 el61. *Astrophys. J.* 632, L45–L48.

Canales, J.P., Detrick, R.S., Lin, J., Collins, J.A., and Toomey, D.R. (2000) Crustal and upper mantle seismic structure beneath the rift mountains and across a nontransform offset at the Mid-Atlantic Ridge (35 degrees N) *J. Geophys. Res.* 105, B2 2699–2719.

Charlou, J.L., Fouquet, Y., Bougault, H., Donval, J.P., Etoubleau, J., Jean-Baptiste, P., Dapoigny, A., Appriou, P., and Rona, P.A. (1998) Intense CH_4 plumes generated by serpentinization of ultramafic rocks at the intersection of the 15°20′N fracture zone and the Mid-Atlantic Ridge. *Geochim. Cosmochim. Acta* 62, 2323–2333.

Charlou, J.L., Donval, J.P., Fouquet, Y., Jean-Baptiste, P., and Holm, N. (2002) Geochemistry of high H_2 and CH_4 vent fluids issuing from ultramafic rocks at the Rainbow hydrothermal field (36°14′N, MAR) *Chem. Geol.* 191, 345–359.

Crone, T.J. and Wilcock, W.S.D. (2005) Modeling the effects of tidal loading on mid-ocean ridge hydrothermal systems. *Geochemistry Geophysics Geosystems* 6, Q07001.

Delsanti, A.C. and Jewitt, D.C. (2006) The Solar System beyond the planets. In *Solar System Update*, edited by P. Blondel and J. Mason, Springer-Praxis, Berlin, pp. 267–294.

deMartin, B., Hirth, G., and Evans, B. (2004) Experimental constraints on thermal cracking of peridotite at oceanic spreading centers. In *Mid-Ocean Ridges: Hydrothermal Interactions between the Lithosphere and Oceans, Geophysical Monograph Series 148*, American Geophysical Union, Washington, DC, pp. 167–185.

Douville, E., Charlou, J.L., Oelkers, E.H., Bienvenu, P., Colon, C.F.J., Donval, J.P., Fouquet, Y., Prieur, D., and Appriou, P. (2002) The Rainbow vent fluids (36°14′N, MAR): the influence of ultramafic rocks and phase separation on trace metal content in Mid-Atlantic Ridge hydrothermal fluids. *Chem. Geol.* 184, 37–48.

Dziewonski, A.M. and Anderson, D.L. (1981) Preliminary reference Earth model. *Physics of the Earth and Planetary Interiors* 25, 297–356.

Evans, A. and Clarke, D. (1980) Residual stresses and microcracking induced by thermal contraction inhomogeneity. *Thermal Stress in Severe Environments*, Plenum Press, New York, pp. 629–648.

Fisher, A.T. (1998) Permeability within basaltic oceanic crust. *Rev. Geophys.* 36, 143–182.

Fisher, A.T. and Becker, K. (2000) Channelized fluid flow in oceanic crust reconciles heat-flow and permeability data. *Nature* 403, 71–74.

Fisk, M.R. and Giovannoni, S.J. (1999) Sources of nutrients and energy for a deep biosphere on Mars. *J. Geophys. Res.* 104, 11805–11815.

Formisano, V., Atreya, S., Encrenaz, T., Ignatiev, N., and Giuranna, M. (2004) Detection of methane in the atmosphere of Mars. *Science* 306, 1758–1761.

Fredrich, J.T. and Wong, T.F. (1986) Micromechanics of thermally induced cracking in 3 crustal rocks. *J. Geophys. Res.* 91, 12743–12764.

Gold, T. (1992) The deep, hot biosphere. *Proc. Natl. Acad. Sci. U.S.A.* 89, 6045–6049.

Hirth, G. and Kohlstedt, D.L. (1995) Experimental constraints on the dynamics of the partially molten uppermantle. 2. Deformation in the dislocation creep regime. *J. Geophys. Res.* 100, 15441–15449.

Hofmeister, A. (1999) Mantle values of thermal conductivity and the geotherm from phonon lifetimes. *Science* 283, 1699–1706.

Hussmann, H. and Spohn, T. (2004) Thermal-orbital evolution of Io and Europa. *Icarus* 171, 391–410.

Hussmann, H., Sohl, F., and Spohn, T. (2006) Subsurface oceans and deep interiors of medium-sized outer planet satellites and large trans-neptunian objects. *Icarus* 185, 258–273.

Jacob, C.E. (1940) On the flow of water in an elastic artesian aquifer. *Transactions of the American Geophysical Union* 21, 574–586.

Jakosky, B.M. and Shock, E.L. (1998) The biological potential of Mars, the early Earth, and Europa. *J. Geophys. Res.* 103, 19359–19364.

Janecky, D. and Seyfried, W. (1986) Hydrothermal serpentinization of peridotite within the oceanic-crust—experimental investigations of mineralogy and major element chemistry. *Geochim. Cosmochim. Acta* 50, 1357–1378.

Kargel, J.S., Kaye, J.Z., Head, J.W., III, Marion, G.M., Sassen, R., Crowley, J.K., Ballesteros, O.P., Grant, S.A., and Hogenboom, D.L. (2000) Europa's crust and ocean: origin, composition, and the prospects for life. *Icarus* 148, 226–265.

Kelley, D.S. and Früh-Green, G.L. (2001) Volatile lines of descent in submarine plutonic environments: insights from stable isotope and fluid inclusion analyses. *Geochim. Cosmochim. Acta* 65, 3325–3346.

Kelley, D.S., Karson, J.A., Früh-Green, G.L., Yoerger, D.R., Shank, T.M., Butterfield, D.A., Hayes, J.M., Schrenk, M.O., Olson, E.J., Proskurowski, G., Jakuba, M., Bradley, A., Larson, B., Ludwig, K., Glickson, D., Buckman, K., Bradley, A.S., Brazelton, W.J., Roe, K., Elend, M.J., Delacour, A., Bernasconi, S.M., Lilley, M.D., Baross, J.A., Summons, R.T., and Sylva, S.P. (2005) A serpentinite-hosted ecosystem: the Lost City hydrothermal field. *Science* 307, 1428–1434.

Kerr, R.A. (2005) Planetary science: Cassini catches mysterious hot spot on icy-cold Enceladus. *Science* 309, 859–860.

Krasnopolsky, V.A. (2005) A sensitive search for SO_2 in the martian atmosphere: implications for seepage and origin of methane. *Icarus* 178, 487–492.

Leger, A., Selsis, F., Sotin, C., Guillot, T., Despois, D., Mawet, D., Ollivier, M., Labeque, A., Valette, C., and Brachet, F. (2004) A new family of planets? "Ocean-Planets." *Icarus* 169, 499–504.

Link, L.S., Jakosky, B.M., and Thyne, G.D. (2005) Biological potential of low-temperature aqueous environments on Mars. *Int. J. Astrobiology* 4, 155–164.

Lister, C.R.B. (1974) Penetration of water into hot rock. *Geophysical Journal of the Royal Astronomical Society* 39, 465–509.

Lowell, R.P. and DuBose, M. (2005) Hydrothermal systems on Europa. *Geophys. Res. Lett.* 32, L05202.

Lyons, W.B., Welch, K.A., Snyder, G., Olesik, J., Graham, E.Y., Marion, G.M., and Poreda, R.J. (2005) Halogen geochemistry of the McMurdo Dry Valleys lakes, Antarctica: clues to the origin of solutes and lake evolution. *Geochim. Cosmochim. Acta* 69, 305–323.

Martin, B. and Fyfe, W.S. (1970) Some experimental and theoretical observations on kinetics of hydration reactions with particular reference to serpentinization. *Chem. Geol.* 6, 185–202.

Martin, J. and Lowell, R. (2000) Precipitation of quartz during high-temperature, fracture-controlled hydrothermal upflow at ocean ridges: equilibrium versus linear kinetics. *J. Geophys. Res.* 105, 869–882.

McCollom, T.M. and Seewald, J.S. (2001) A reassessment of the potential for reduction of dissolved CO_2 to hydrocarbons during serpentinization of olivine. *Geochim. Cosmochim. Acta* 65, 3769–3778.

McCollom, T.M. and Shock, E.L. (1997) Geochemical constraints on chemolithoautotrophic metabolism by microorganisms in seafloor hydrothermal systems. *Geochim. Cosmochim. Acta* 61, 4375–4391.

McCollom, T.M. and Shock, E.L. (1998) Fluid-rock interactions in the lower oceanic crust: thermodynamic models of hydrothermal alteration. *J. Geophys. Res.* 103, 547–575.

McCollom, T.M., Ritter, G., and Simoneit, B.R.T. (1999) Lipid synthesis under hydrothermal conditions by Fischer-Tropsch-type reactions. *Orig. Life Evol. Biosph.* 29, 153–166.

McCord, T.B. and Sotin, C. (2005) Ceres: evolution and current state. *J. Geophys. Res.* 110, E05009.

McKinnon, W.B. and Zolensky, M.E. (2003) Sulfate content of Europa's ocean and shell: evolutionary considerations and some geological and astrobiological implications. *Astrobiology* 3, 879–897.

Moody, J. (1976) Serpentinization: a review. *Lithos* 9, 125–138.

Moore, W.B. and Schubert, G. (2000) The tidal response of Europa. *Icarus* 147, 317–319.

Murray, C.D. and Dermott, S.F. (1998) *Solar System Dynamics,* Cambridge University Press, Cambridge.

Neal, C. and Stanger, G. (1983) Hydrogen generation from mantle source rocks in Oman. *Earth Planet. Sci. Lett.* 66, 315–320.

Nesbitt, H. and Bricker, O. (1978) Low-temperature alteration processes affecting ultramafic bodies. *Geochim. Cosmochim. Acta* 42, 403–409.

O'Hanley, D.S. (1992) Solution to the volume problem in serpentinization. *Geology* 20, 705–708.

Oze, C. and Sharma, M. (2005) Have olivine, will gas: serpentinization and the abiogenic production of methane on Mars. *Geophys. Res. Lett.* 32, L10203.

Pedersen, K. (2000) Exploration of deep intraterrestrial microbial life: current perspectives. *FEMS Microbiol. Lett.* 185, 9–16.

Pendleton, Y.J. and Allamandola, L.J. (2002) The organic refractory material in the diffuse interstellar medium: mid-infrared spectroscopic constraints. *Astrophysical Journal Supplement Series* 138, 75–98.

Porco, C.C., Helfenstein, P., Thomas, P.C.T., Ingersoll, A.P., Wisdom, J., West, R., Neukum, G., Denk, T., Wagner, R., Roatsch, T., Kieffer, S. Turtle, E., McEwen, A., Johnson, T.V., Rathbun, J., Veverka, J., Wilson, D., Perry, J., Spitale, J., Brahic, A., Burns, J.A., DelGenio, A.D., Dones, L., Murray, C.D., and Squyres, S. (2006) Cassini observes the active south pole of Enceladus. *Science* 311, 1393–1401.

Rabinowitz, D.L., Barkume, K., Brown, M.E., Roe, H., Schwartz, M., Tourtellotte, S., and Trujillo, C. (2006) Photometric observations constraining the size, shape, and albedo of 2003 EL61, a rapidly rotating, Pluto-sized object in the Kuiper Belt. *Astrophys. J.* 639, 1238–1251.

Raymond, S., Mandel, A., and Sigurdsson, S. (2006) Exotic earths: forming habitable worlds with giant planet formation. *Science* 313, 1413–1416.

Rosing, M.T. (1999) 13C-depleted carbon microparticles in >3700-Ma sea-floor sedimentary rocks from west Greenland. *Science* 283, 74–76.

Schroeder, T., John, B., and Frost, B. (2002) Geologic implications of seawater circulation through peridotite exposed at slow-spreading mid-ocean ridges. *Geology* 30, 367–370.

Schubert, G., Spohn, T., and Reynolds, R. (1986) Thermal histories, compositions and internal structures of the moons of the Solar System. In *Satellites*, University of Arizona Press, Tucson, pp. 224–292.

Schulte, M., Blake, D., Hoehler, T., and McCollom, T. (2006) Serpentinization and its implications for life on the early Earth and Mars. *Astrobiology* 6, 364–376.

Sclater, J., Jaupart, C., and Galson, D. (1980) The heat flow through oceanic and continental crust and the heat loss of the Earth. *Reviews of Geophysics and Space Physics* 18, 269–311.

Segatz, M., Spohn, T., Ross, M.N., and Schubert, G. (1988) Tidal dissipation, surface heat flow and figures of viscoelastic models of Io. *Icarus* 75, 187–206.

Seyfried, W. and Dibble, W. (1980) Seawater-peridotite interaction at 300 degrees C and 500 bars: implications for the origin of oceanic serpentites. *Geochim. Cosmochim. Acta* 44, 309–321.

Shock, E.L. (2004) Quenching, mixing, reaction progress, and the hydrothermal support of the biosphere. *Geochim. Cosmochim. Acta* 68, A259–A259.

Sinha, M. and Evans, R. (2004) Geophysical Constraints Upon the Thermal Regime of the Ocean Crust. In *Mid-Ocean Ridges: Hydrothermal Interactions Between the Lithosphere and Oceans*, edited by C.R. German, J. Lin, and L.M. Parson, AGU Press, Washington, DC.

Skelton, A., Whitmarsh, R., Arghe, F., Crill, P., and Koyi, H. (2005) Constraining the rate and extent of mantle serpentinization from seismic and petrological data: implications for chemosynthesis and tectonic processes. *Geofluids* 5, 153–164.

Sleep, N., Meibom, A., Fridriksson, T., Coleman, R., and Bird, D. (2004) H_2-rich fluids from serpentinization: geochemical and biotic implications. *Proc. Natl. Acad. Sci. U.S.A.* 101, 12818–12823.

Spencer, J.R., Pearl, J.C., Segura, M., Flasar, F.M., Mamoutkine, A., Romani, P., Buratti, B.J., Hendrix, A.R., Spilker, L.J., and Lopes, R.M.C. (2006) Cassini encounters Enceladus: background and the discovery of a south polar hot spot. *Science* 311, 1401–1405.

Spohn, T. and Schubert, G. (2003) Oceans in the icy galilean satellites of Jupiter? *Icarus* 161, 456–467.

Stein, C., Stein, S., and Pelayo, A. (1995) Heat flow and hydrothermal circulation. In *Seafloor Hydrothermal Systems, Geophysical Monograph Series, Vol. 91*, AGU, Washington, DC, pp. 425–445.

Tobie, G., Mocquet, A., and Sotin, C. (2005a) Tidal dissipation within large icy satellites: applications to Europa and Titan. *Icarus* 177, 534–549.

Tobie, G., Grasset, O., Lunine, J.I., Mocquet, A., and Sotin, C. (2005b) Titan's internal structure inferred from a coupled thermal-orbital model. *Icarus* 175, 496–502.

Turcotte, D.L. and Schubert, G. (1982) *Geodynamics: Applications of Continuum Physics to Geological Problems*, Wiley, New York.

van der Kamp, G. and Gale, J.E. (1983) Theory of Earth tide and barometric effects in porous formations with compressible grains. *Water Resour. Res.* 19, 538–544.

Van Kranendonk, M. (2006) Volcanic degassing, hydrothermal circulation and the flourishing of life on Earth: a review of the evidence from c. 3490–3240 Ma rocks of the Pilbara Supergroup, Pilbara Craton, Western Australia. *Earth Science Review* 74, 197–240.

Wang, K. and Davis, E.E. (1996) Theory for the propagation of tidally induced pore pressure variations in layered subseafloor formations. *J. Geophys. Res.* 101 B5, 11483–11495.

Wang, K., van der Kamp, G., and Davis, E.E. (1999) Limits of tidal energy disspation by fluid flow in subsea formations. *Geophys. J. Int.* 139, 763–768.

Wegner, W. and Ernst, W. (1983) Experimentally determined hydration and dehydration reaction rates in the system $MgO\text{-}SiO_2\text{-}H_2O$. *Am. J. Sci.* 283A, 151–180.

Weiss, B.P. and Ingersoll, A.P. (2000) Cold spots in the martian polar regions: evidence of carbon dioxide depletion? *Icarus* 144, 432–435.

Wetzel, L.R. and Shock, E.L. (2000) Distinguishing ultramafic- from basalt-hosted submarine hydrothermal systems by comparing calculated vent fluid compositions. *J. Geophys. Res.* 105, 8319–8340.

Wogelius, R. and Walther, J. (1992) Olivine dissolution kinetics at near-surface conditions. *Chem. Geol.* 97, 101–112.

Zimmer, C., Khurana, K.K., and Kivelson, M.G. (2000) Subsurface oceans on Europa and Callisto: constraints from Galileo magnetometer observations. *Icarus* 147, 329–347.

Zimmerman, R., Somerton, W., and King, M. (1986) Compressibility of porous rocks. *J. Geophys. Res.* 91, 12765–12777.

Zolotov, M.Y. and Shock, E.L. (2003) Energy for biologic sulfate reduction in a hydrothermally formed ocean on Europa. *J. Geophys. Res.* 108, 5022.

Zolotov, M.Y. and Shock, E.L. (2004) A model for low-temperature biogeochemistry of sulfur, carbon, and iron on Europa. *J. Geophys. Res.* 109, E06003, doi: 10.1029/2003JE002194.

Address reprint requests to:
Steve Vance
Jet Propulsion Laboratory
4800 Oak Grove Drive
Pasadena, CA 91109

E-mail: svance@ess.washington.edu